Journal of Applied Physics

Effect of texture on the electrical and electrocaloric properties of $0.90Pb(Mg_{1/3}Nb_{2/3})O_3$–$0.10PbTiO_3$ relaxor ceramics

Cite as: J. Appl. Phys. **128**, 084102 (2020); https://doi.org/10.1063/5.0003296
Submitted: 31 January 2020 • Accepted: 06 August 2020 • Published Online: 24 August 2020

Ebru Mensur-Alkoy, M. Baris Okatan, Ecem Aydin, et al.

Journal of Applied Physics ARTICLE scitation.org/journal/jap

Effect of texture on the electrical and electrocaloric properties of $0.90Pb(Mg_{1/3}Nb_{2/3})O_3$–$0.10PbTiO_3$ relaxor ceramics

Cite as: J. Appl. Phys. **128**, 084102 (2020); doi: 10.1063/5.0003296
Submitted: 31 January 2020 · Accepted: 6 August 2020 ·
Published Online: 24 August 2020

Ebru Mensur-Alkoy,[1,a)] M. Baris Okatan,[2] Ecem Aydin,[1] Yusuf Kilic,[1] I. Burc Misirlioglu,[3,4] and Sedat Alkoy[1]

AFFILIATIONS

[1]Department of Materials Science and Engineering, Gebze Technical University, 41400 Kocaeli, Turkey
[2]Department of Materials Science and Engineering, Izmir Institute of Technology, Gulbahce/Urla, 35430 Izmir, Turkey
[3]Faculty of Engineering and Natural Sciences, Sabanci University, Orhanli/Tuzla, 34956 Istanbul, Turkey
[4]Sabanci University Nanotechnology Research and Application Center, Orhanli/Tuzla, 34956 Istanbul, Turkey

Note: This paper is part of the Special Topic on: Multicalorics.
[a)]**Author to whom correspondence should be addressed:** ebrualkoy@gtu.edu.tr. **Tel.:** +90(262) 605 2668

ABSTRACT

Functional properties of ferroelectric compositions depend strongly on the type of stable crystalline phase at a given temperature and texturing. In addition to defining a governing crystallographic axis among the grains with respect to a global reference axis, texturing in these systems is also often meant to imply the relationship between an external applied field and the polar axis. Here, we synthesize randomly oriented and $\langle 001 \rangle_{pc}$ textured $0.90Pb(Mg_{1/3}Nb_{2/3})O_3$–$0.10PbTiO_3$ solid solutions that fall into the relaxor category. A >95% degree of $\langle 001 \rangle_{pc}$ texturing was achieved by the use of single crystal $BaTiO_3$ template crystallites whose volume fraction does not exceed 5% of the entire sample volume. Electrical measurements made on random and textured samples reveal the impact of texture on the hysteresis and the dielectric response. A Curie–Weiss analysis of the temperature dependent dielectric data shows the degree of relaxor behavior in random and textured samples. As similar compositions have recently been getting interest for electrothermal management applications, we compute the electrocaloric (EC) response of the random and textured samples using indirect methods followed by an estimation of the EC response with a subsequent thermodynamic analysis to shed light on the effect of texture on the observed differences between the textured and the random oriented samples. We finally compare and contrast on the desirability of texturing in these systems for use as EC components for thermal management applications.

I. INTRODUCTION

Among the solid-state temperature control approaches (Greco *et al.*, 2019), tailoring the electrocaloric (EC) response of ferroelectric materials has entered the agenda of many research and technology groups for the convenience with which one can induce temperature changes in the ferroelectric lattice (Valant, 2012). The ease of the application of an electric field to induce the temperature change in the ferroelectric lattice allows designing devices with compact and simple geometries compatible with many applications requiring thermal management (Fulanovic *et al.*, 2017). In the pursuit of advancing EC device design, recent reports by Mischenko *et al.* (2006) and Lu *et al.* (2010) on ferroelectric thin films demonstrated that bias voltages of only several volts appear to suffice in driving temperature changes amounting to several degrees, exceeding 10 °C in some rare cases. One restriction for thin films, however, emanates from the very definition of the system: a thin film volume is often extremely small to effectively remove heat from the system to be thermally managed despite the attractive temperature changes these systems can possess under bias.

The use of ferroelectric materials in bulk state, fabricated and shaped in a desired geometry, allows for a larger volume to exchange heat with the system to be thermally managed. This, however, is possible at the expense of lower temperature gradients as quite high bias values are needed to reach the temperatures reported for thin

films. In spite of this apparent difficulty, the integration of ferroelectrics into the EC device design in bulk form remains attractive. A number of studies (Qian *et al.*, 2014 and Sanlialp *et al.*, 2016) have focused on engineering the composition of ferroelectrics to maximize the temperature change in the lattice under electric fields falling into ranges pronounced as low-to-moderate for these materials (10–30 kV/m). If one thinks of the EC effect (ECE) as a consequence of the entropy change one generates via enforcing order upon the ferroelectric dipoles under an applied field at a given temperature, an intuitive approach to maximize the ECE is to work with ferroelectric compositions allowing for several structural variants. Following such an intuition, one could expect a greater difference of entropy between the states of "electric field induced ordering" and "zero field state with variants," corresponding to a greater amount of heat generation between applied field and zero field states. With this in mind, we decided to conduct a systematic study on the effect of texture on the EC response of a relaxor composition crystallizing in rhombohedral symmetry, namely, $0.90Pb(Mg_{1/3}Nb_{2/3})O_3$–$0.10PbTiO_3$ (0.90PMN–0.10PT). The 0.90PMN–0.10PT composition was chosen because the ferroelectric–paraelectric phase transition temperature is very close to room temperature (RT), which would be a critical advantage for possible EC device applications. That the Curie temperature of this system is near room temperature (RT) brings about the expectation of a rather high ECE as the pyroelectric coefficient, which the ECE is a function of, displays the maximum near this temperature.

Being a first rank tensor property (Newnham, 2005), the ECE is expected to demonstrate an anisotropy in non-centrosymmetric ferroelectric materials. However, there are very few reports on the anisotropy of ECE in the literature (Valant, 2012). The effect of anisotropy on the ECE was investigated in single crystals of 0.76PMN–0.24PT by Zhang *et al.* (2017), where distinctively different values of EC coefficients with different temperature dependent behavior have been measured along the [100], [110], and [111] directions. Sebald *et al.* (2006) have investigated the ECE of 0.75PMN–0.25PT crystals and compared the results with random ceramics of the same composition. A clear anisotropy has again been observed in the properties with changing crystallographic direction. The effect of electrocaloric anisotropy in lead-free strontium barium niobate SBN75 ($Sr_{0.75}Ba_{0.25}Nb_2O_6$) based uniaxial relaxor ferroelectric single crystals with tetragonal tungsten bronze structure has also been reported by Goupil *et al.* (2014). However, it is well known that single crystals are usually considered too expensive for mass-produced device applications. Thus, it would be a preferable approach to obtain an anisotropy in polycrystalline ceramics through texture development (Messing *et al.*, 2017). However, to the best of our best knowledge, the effect of EC anisotropy in textured ceramics has not been previously reported in the literature. Thus, in the current study, highly $\langle 001 \rangle_{pc}$ oriented 0.90PMN–0.10PT ceramics of high purity were successfully synthesized with a high texture fraction (>95%) using $BaTiO_3$ (BT) template particles, and the effect of crystallographic anisotropy on the EC performance of textured ceramics is being reported for the first time, Additionally, we employed the Landau theory of phase transitions with the phenomenological coefficients reported for PMN–PT in order to shed light on the possible effect of texture on the composition of interest.

II. EXPERIMENTAL

Ceramic powders with $0.90Pb(Mg_{1/3}Nb_{2/3})O_3$–$0.10PbTiO_3$ (0.90PMN–0.10PT) composition were synthesized by the solid-state calcination method. The Columbite method was followed, where $MgNb_2O_6$ powder was initially synthesized from niobium (V) oxide—Nb_2O_5 (Alfa Aesar, 99.5%)—and magnesium carbonate hydroxide pentahydrate—$(MgCO_3)_4 \cdot Mg(OH)_2 \cdot 5H_2O$ (Sigma Aldrich, 98%)—source powders to eliminate the formation of undesirable secondary phases in PMN–PT. The detailed information about processing of $MgNb_2O_6$ powder has been given in our previous papers (Berksoy-Yavuz, 2018). In addition to the $MgNb_2O_6$ powder, lead (II) carbonate basic—$(PbCO_3)_2.Pb(OH)_2$ (Sigma Aldrich)—and titanium dioxide—TiO_2 (Degussa, P25)—were used as lead and titanium sources, respectively, in the synthesis of PMN–PT powders. The powder mixture was calcined at 850 °C for 4 h with a ramp rate of 5 °C/min. Additionally, plate-like BT template particles were synthesized with the molten salt synthesis (MSS) and topochemical microcrystal conversion (TMC) methods. The details of the BT template synthesis route followed in this study were reported in the literature (Liu *et al.*, 2007 and Berksoy-Yavuz *et al.*, 2019). Slurries for the tape casting process were prepared from the calcined PMN–PT powders using an organic binder mixture and methyl ethyl ketone (MEK) + ethanol as solvent. All tapes were cast using a doctor blade with 200 μm blade gap and a casting speed of 10 cm/s on a glass substrate. The details of the powder synthesis and tape casting process have been reported in our previous study (Berksoy-Yavuz, 2018). In this study, textured PMN–PT ceramic samples were fabricated by adding 5 vol. % BT templates into the slurries. The ceramics that were fabricated with BT templates following this route were called as textured PMN–PT ceramics (90T). The major (001) surfaces of the templates were aligned parallel to the casting direction, i.e., parallel to the glass plate. After drying at room temperature for 2 h, the green tapes were removed from the glass substrate. The ceramics that were fabricated without any templates following the same route were called as random PMN–PT ceramic (90R). Afterward, the tapes were punched with a green diameter of 16 mm and then 20–40 single tapes were laminated together at 80 °C under uniaxial pressure at 100 MPa. Following that, the green samples were pressed with cold isostatic pressing (CIP) at 150 MPa for 5 min. Finally, the organic content was removed from the green ceramics at 600 °C for 1 h with a heating rate of 1 °C/min and then sintered at 1250 °C for 6 h in air atmosphere with a ramp rate of 5 °C/min. Major surfaces of the sintered samples were ground and polished to form parallel surfaces. The final diameter of the samples was 13.5 mm and thickness of the samples was either 500 μm or 1000 μm. The samples were coated with silver paste electrodes for electrical measurements. Then, the samples were heated to 600 °C with a ramp of 5 °C/min and soaked for 30 min to fire the silver electrodes.

The phase analysis of the powders and ceramics were done by an x-ray diffractometer (XRD) (Bruker D8 Advanced, Germany) using a Cu–K_α radiation ($2\theta = 20°$–$60°$ with a step size of 0.02°). Indexing of the diffraction peaks was done using a pseudo-cubic symmetry notation. The degree of grain orientation along $<001>_{pc}$ in the textured ceramics was calculated from the XRD pattern by

Lotgering's method (1959). The bulk density of sintered samples was determined using the Archimedes' method. The surface and cross-sectional microstructure of the ceramics were examined by a scanning electron microscope (SEM) (Philips XL30 FEI Co., USA). The samples were prepared for the SEM investigation by grinding and polishing, followed by thermal annealing for 30 min at 980 °C. The polarization vs electric field hysteresis loops (P–E) of samples were measured at a 0.5–3.0 Hz frequency range with a Precision LC ferroelectric tester (Radiant Technologies, Inc., USA). The field direction was perpendicular to the tape casting direction and, thus, parallel to the [001] crystallographic axis in the case of textured ceramics. The temperature dependence of dielectric constant (ε_r) and loss tangent ($\tan\delta$) of unpoled samples were measured at 1–100 kHz using a Hioki 3520 LCR meter (Hioki, Japan) from room temperature to 160 °C by heating at 2 °C/min. Electrocaloric response of PMN–PT ceramics was determined indirectly through an inspection of temperature dependent evolution of several P–E loops captured while cooling from 90 °C down to 0 °C.

III. RESULTS AND DISCUSSION

A. Structural and electrical features of random and textured ceramics

The XRD patterns of random and textured ceramics and the BT template particles are shown in Fig. 1. It can be seen that all samples crystallized in the perovskite phase without any visible secondary phases within the detection limits of the diffractometer. In the XRD pattern of the BT template particles, the splitting of the peak at around 45° belonging to (002)/(200) planes was a clear identifier of the tetragonal structure. The random PMN–PT ceramic (90R) had the highest intensity for the $(110)_{pc}$ peak, while

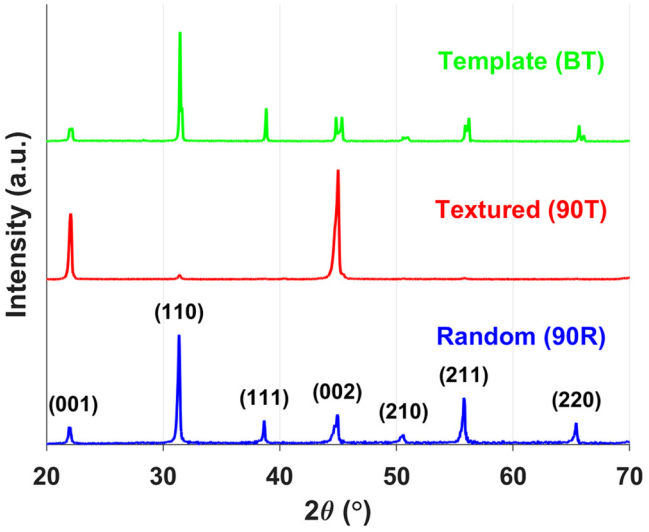

FIG. 1. Comparison of the XRD patterns of textured (90T) and random (90R) samples, and $BaTiO_3$ (BT) templates. The peaks were indexed assuming a pseudo-cubic perovskite structure.

the intensities of (00*l*) peaks increased sharply in textured PMN–PT ceramics (90T). The Lotgering factor, *f*, of textured ceramics was calculated >95%. A closer investigation of the (111) peak of random ceramic at around 39° did not reveal a peak splitting, which would have been a fingerprint of a rhombohedral crystal symmetry. This is in agreement with the literature (Gehring *et al.*, 2003), where zero field neutron scattering measurements on PMN–PT single crystals containing 10%PT revealed a single (111) peak, indicative of a cubic symmetry. Similar results were also obtained by Xu *et al.*, (2003) in PMN–PT single crystals with 20%PT. However, these results did not exclude the presence of a ferroelectric polar order and development of polar nanoregions (PNRs) below the Burns temperature (T_B) in these relaxor systems (Burns and Dacol, 1983). A small external force, such as the application of a small electric field, was reported to lead to a transformation into the rhombohedral phase below T_m (Xu *et al.*, 2003).

After the phase analysis and determination of texture, microstructural features of the random and textured ceramics were investigated and the cross-sectional SEM micrographs of polished and thermally etched surfaces of randomly oriented and textured ceramics are given in Fig. 2. The random ceramics were found to be fairly dense [Fig. 2(a)], whereas the textured samples were observed to contain porosity with sizes <10 μm [Fig. 2(b)], as seen from the micrographs. The density measurements by the Archimedes' technique indicated densities exceeding 96% of the theoretical value for both random and textured samples.

The grain sizes in the random ceramics were <10 μm with a rather uniform grain size distribution [Fig. 2(a)]. The textured ceramics on the other hand had a wider grain size distribution due to the grain growth induced through the BT template particles, where elongated grains containing the BT templates were observed to reach grain sizes up to around 20 μm. The edge-on BT templates embedded in the PMN–PT matrix grains and marked with white arrows in the SEM micrograph were visible with a dark contrast in the micrograph displayed in Fig. 2, and they were found to be well-aligned along the tape casting direction [the horizontal direction in Fig. 2(b)].

In order to compare the effect of texturing and possible microstructural factors on the dielectric response of the samples, we give the dielectric constants (ε_r) and loss tangent ($\tan\delta$) of the 90R and 90T samples with respect to temperature at 1 kHz, 10 kHz and 100 kHz in Figs. 3(a) and 3(d), respectively. The measurements have been taken from unpoled samples during the heating-up ramp. Relaxor behavior was observed in both cases, where a broad and frequency-dependent maximum was observed in the dielectric constant vs temperature behavior. However, this maximum in relaxors does not indicate a transition into a long-range ordered polar state with macroscopic polarization, as it is the case in normal ferroelectrics (Cross, 1987). The observation for the random sample here is in parallel with those initial reports by Viehland (1990) that explain the relaxor behavior on the basis of superparaelectric clusters that yield a collective response under an applied field. Textured samples display the same behavior albeit possessing a structural order imposed by the BT templates. One would have expected a more prominently suppressed dielectric response in a textured sample where the measurement axis is perpendicular to the axis along which strain might be imposed by the

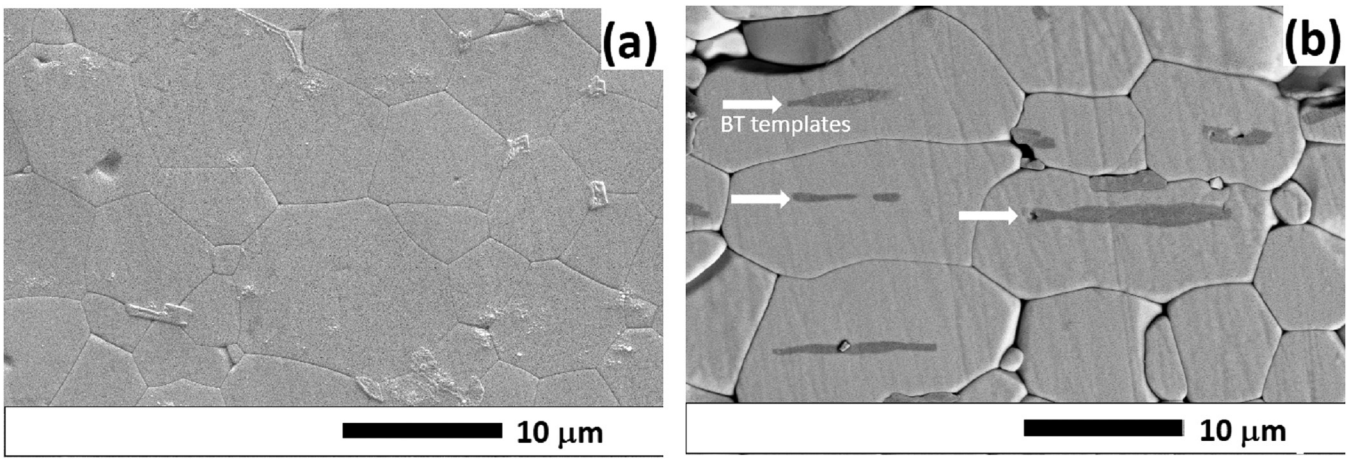

FIG. 2. The cross-sectional SEM micrographs of (a) random (90R) and (b) textured (90T) ceramics.

templates. This claim is discussed in light of various possible mechanisms in the proceeding paragraphs. Therefore, despite the apparent strong texture confirmed by the >95% Lotgering factor, it is possible to conclude that the main mechanism behind the relaxor nature is rather strain or clamping insensitive, at least for the composition of interest herein.

The above argument is supported by the observation where the temperatures at which a dielectric constant maximum was observed (T_m) were similar at every measurement frequency for random and textured ceramics, which also means that the BT templates or the development of crystallographic texture did not create any shift in the T_m measured as 46 °C at 100 kHz, similar to the values reported in the literature by Yimnirun (2009) and Vrabelj *et al.* (2016). In another work, Richter *et al.* (2008) observed a downward shift in the Curie temperature of the textured PMN–32PT ceramic, and it was attributed to the partial dissolution of the BT templates and diffusion of Ba ions into the matrix. In our case, the BT templates were clearly observable in the SEM micrographs, with no apparent dissolution, and it is our assumption that there was no significant diffusion to induce a change in the Curie temperature.

Textured samples, on the other hand, displayed a broader transition, as shown in Fig. 3(d), and the maximum dielectric constant at the transition was visibly lower ($\varepsilon_{max} = 14\,120$ and $T_m = 38$ °C at 1 kHz) compared to the random ceramics ($\varepsilon_{max} = 18\,827$ and $T_m = 40$ °C at 1 kHz). A similar trend of decreasing peak value of textured ceramics compared to the random one has been observed by Richter *et al.* (2008) in their study on PMN–32PT and by our group (Berksoy-Yavuz *et al.*, 2018). This decrease could be attributed to four different and competing reasons: (i) The elastoelectric composite effect where the dielectric constant is expected to decrease due to the presence of a low dielectric constant BT templates in 5 vol. % ratio (Messing *et al.*, 2004 and Berksoy-Yavuz *et al.*, 2018). (ii) The higher presence of porosity in the textured ceramics compared to the random case is also believed to be another culprit for the observation of lower dielectric constant values with the developing texture. The porosities would have contributed a zero polarization; hence, a much lower dielectric constant compared to the dense ceramics is expected. Textured samples are reported to exhibit relatively higher porosity due to the insufficient packing of larger, elongated grains. Thus, porosities may also lead to a decrease in the total dielectric constant of the textured ceramics (Messing *et al.*, 2004). (iii) Additionally, keeping in mind the nature of the relaxor composition, dielectric response is intimately connected with "flexibility of polarization" inside the lattice (Viehland *et al.*, 1990). If one evaluates a relaxor composition near the transition temperature (as is the case for our samples having a Curie point near room temperature) as composed of superparaelectric regions free to rotate in the random (90R) sample, a template crystal will be expected to "reduce this flexibility"; hence, a lower polarization response with an applied field (dP/dE) can be expected. Such an effect will certainly be felt stronger by the lattice near the template particles and will likely vanish toward the stress- and clamping-free surfaces, therefore resulting in a relative loss in the dielectric response with respect to the 90R sample. (iv) Finally, the anisotropy of a second rank tensor property in non-cubic symmetries was also considered a possible reason. PMN–10PT is expected to assume a rhombohedral symmetry. A crystal with a rhombohedral symmetry is expected to have three non-zero dielectric constant coefficients, namely K_{11}, K_{22}, and K_{33}. Since $K_{11} = K_{22}$ in uniaxial symmetries such as rhombohedral systems, then there will be two independent permittivity values along the principal axis perpendicular to each other (K_{33} and K_{11}). K_{33} would be along the high symmetry axis, i.e., the "c axis" of the rhombohedral crystal (or the $[111]_{pc}$ direction using the cubic symmetry notation). Thus, the value measured along the $[111]_{pc}$ direction ($K_{[111]}$) would purely yield K_{33}. K_{11} would be perpendicular to the c axis of the rhombohedral structure. Reverting to the parent cubic symmetry notation, K_{11} would lie along a direction which is between $[\bar{1}\bar{1}1]_{pc}$ and $[001]_{pc}$ directions. Thus, the value measured along $[001]_{pc}$ direction ($K_{[001]}$) would have contributions from both K_{11} and K_{33}. In fact, the value of $K_{[001]}$ can be calculated according to the

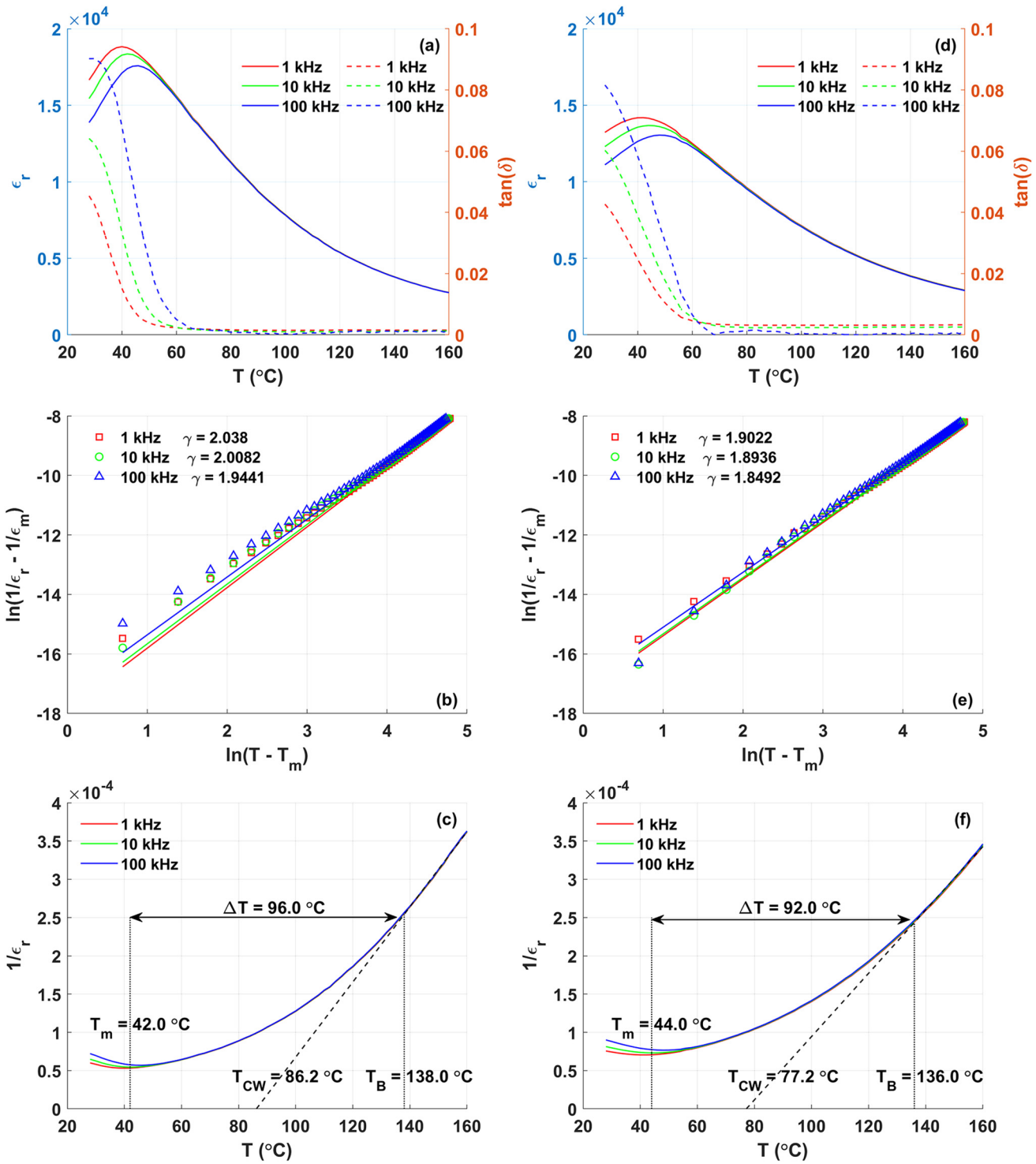

FIG. 3. Temperature dependent dielectric properties of (a)–(c) random (90R) and (d)–(f) textured (90T) ceramics. (a) and (d) Dielectric constant (solid lines) and loss tangent (dashed lines) vs temperature, (b) and (e) the $\ln(1/\varepsilon_r - 1/\varepsilon_m)$ vs $\ln(T - T_m)$ plots, and (c) and (f) the temperature dependence of the inverse of permittivity measured at various frequencies.

following equation in spherical coordinates for the rhombohedral symmetry, $K_{[001]} = K_{11}\sin^2(\theta) + K_{33}\cos^2(\theta)$ where $\theta = 54.7°$ for the specific case of [111] and [001] directions (Newnham, 2005). Then, depending on the specific values of permittivity of the single crystal along principal axes (K_{11} and K_{33}), and whether $K_{11} > K_{33}$ or $K_{11} < K_{33}$, the measured values of $K_{[111]}$ or $K_{[001]}$ may be higher, as it was reported by Wang *et al.* (2005) for 0.90PMN–0.10PT single crystals.

In the case of random ceramics, on the other hand, since the orientation of grains is random, the measured dielectric constant along an arbitrary direction (K'_{meas}) would basically be the numerical average of the principal relative permittivities according to the equation $\langle K'_{meas}\rangle = \frac{1}{3}(K_{11} + K_{22} + K_{33})$ (Newnham, 2005). Solutions of the two equations given above for numerical values that K_{11} and K_{33} may take clearly indicate that for the specific $\theta = 54.7°$ case, a significant difference would not be observed between the relative permittivity values of the random case (K'_{meas}) compared to $K_{[001]}$ of the textured one because of anisotropy. Thus, the difference that was observed in the current study cannot be attributed to the anisotropy. However, the same analysis indicated that other crystallographic directions with $\theta \neq 54.7°$ do create a significant difference. Additionally, the textured ceramic would have higher relative permittivity values compared to the random case, when the $K_{33} > K_{11}$ and the texture was along $[111]_{pc}$ direction, instead of the $[001]_{pc}$ direction for the rhombohedral symmetry.

In regular and commensurate ferroelectrics, the temperature dependence of the dielectric constant above the dielectric constant maximum can be described with the Curie–Weiss law (Uchino and Nomura, 1982). However, 0.90PMN–0.10PT is known (Yimnirun, 2009) to exhibit relaxor-like characteristics, and as it is obviously seen from Figs. 3(a) and 3(d), both the random and textured 0.90PMN–0.10PT exhibited the characteristics of the relaxor ferroelectric materials such as diffuse phase transition behavior, a frequency-dependent shift of the temperature of the dielectric constant maximum, and a strong deviation from the Curie–Weiss behavior at high temperatures (Dai *et al.*, 1994). Thus, the temperature dependent dielectric behavior of the PMN–PT ceramics in the current study are expected to deviate from the Curie–Weiss law, but this deviation can be described with a modified relationship (Uchino, 1982; Kaya *et al.*, 2018; and Cakmak *et al.*, 2020),

$$\frac{1}{\varepsilon_r} - \frac{1}{\varepsilon_m} = \frac{(T - T_m)^\gamma}{C}. \quad (1)$$

In this relationship, the ε_m is the maximum value of the dielectric constant, the T_m is the temperature of the dielectric constant maximum, C is the Curie constant, and γ is the degree of broadening or diffusiveness of the phase transition. γ ranges from 1 in normal ferroelectrics to 2 in relaxors. This relationship was used in the analyses of the temperature dependence of dielectric permittivity of 0.90PMN–0.10PT ceramics in the current study. The γ parameter was determined by curve fitting to data represented on a linear scale and then the resulting fits are drawn in log–log plots as given in Figs. 3(b) and 3(e). The γ value was calculated as 1.94 for 90R and 1.85 for 90T at 100 kHz. These values indicate a relaxor dominant character for both ceramics and agree with the literature (Yimnirun, 2009). Thus, the inclusion of BT templates with a normal ferroelectric behavior or the development of crystallographic texture did not cause a meaningful change in the relaxor behavior of the 0.90PMN–0.10PT ceramics.

The deviation from the Curie–Weiss behavior was also demonstrated in the temperature dependence of the inverse permittivity plot given in Figs. 3(c) and 3(f) for 90R and 90T, respectively. The dashed lines in the figures are used to extrapolate the deviation from the Curie–Weiss behavior at high temperatures. The deviation starts at the T_B, which was identified with a fine vertical line in the figures. The T_B of the random ceramics was determined as 138 °C, whereas the T_B of the textured ceramics was determined as 136 °C at 10 kHz. These results also confirm the relaxor behavior of both the random and textured ceramics. The span of temperature difference between the T_m and T_B, i.e., ΔT was found to decrease with the texture. This was believed to arise as a result of addition of the 5 vol. % BT template phase, which is a normal ferroelectric, and thus it is understandable to observe a decrease in relaxor behavior with texturing.

Although Eq. (1) is widely used in the literature to analyze the diffuseness of the dielectric behavior, it was also reported (Bokov *et al.*, 2003; 2005; Wang *et al.*, 2005; Hino *et al.*, 2011; and Liu *et al.*, 2020) to contain an inherent deficiency since frequency-dependent parameters such as T_m and ε_m are used in the estimation of the degree of diffuseness. This in return lends a frequency-dependence to the parameter γ and may not be entirely suitable for the analysis of the static dielectric behavior. A quadratic relationship presented in Eq. (S1) in the supplementary material was proposed to analyze the dielectric behavior of relaxor materials above T_m using a shape parameter δ (Bokov *et al.*, 2003). It was used in various relaxor ferroelectric systems including PMN–PT (Wang *et al.*, 2005 and Bokov *et al.*, 2005). Dielectric constant data given in Figs. 3(a) and 3(d) were re-analyzed, and the results are presented and discussed in the supplementary material and in Figs. S1–S4. The γ parameter in this analysis was found to be equal to 2.52 and 2.42 for random and textured ceramics, respectively. Since, these values deviated drastically away from the expected quadratic ($\gamma = 2$) dependence for relaxor materials, it raised questions about the applicability of this empirical expression to our data, and thus, it was not used in the main text, but it was included in the supplementary material, nevertheless.

A comparison of the typical polarization vs electric field (P–E) hysteresis loops of random and textured samples measured at 0 °C and 25 °C using a measurement frequency of 0.5 Hz and under an electric field of 40 kV/cm is given in Fig. 4(a). Hysteresis loops have also been measured at various frequencies ranging from 0.5 Hz up to 3 Hz, and they have all exhibited similar behavior for both random and textured samples. From Fig. 4(a), the remanent (P_r) and maximum (P_{max}) polarization values as well as the coercive electric field (E_c) of the random sample obtained from the measurement taken at 0 °C are higher than the values observed at 25 °C. This is actually an expected behavior in the relaxor ferroelectric PMN–PT system. In relaxor systems, PNRs are observed below the T_B (Burns and Dacol, 1983), which is well above the T_m (Shvartsman and Kholkin, 2007). The formation of these PNRs is attributed to the inherent compositional disorder in PMN arising from the B-site cations Mg^{2+} and Nb^{5+}. However, in the case of

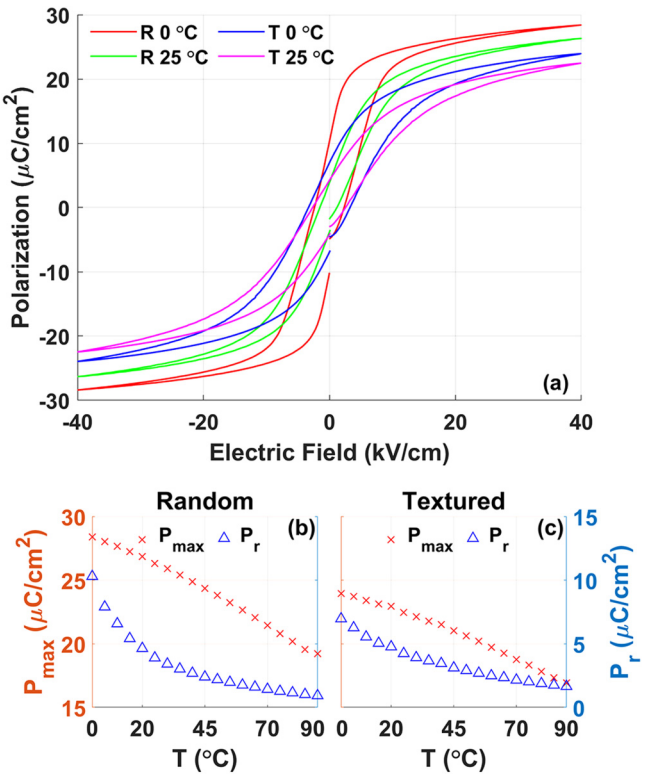

FIG. 4. (a) Electric field induced polarization graphs of random and textured samples at RT and 0 °C. Variation of the remanent (E = 0) and maximum polarization (E = 40 kV/cm) with respect to temperature for (b) random and (c) textured ceramics.

PMN–PT, a second transition temperature has also been reported (Viehland *et al.*, 1990 and Song *et al.*, 2005). Viehland *et al.* (1990) treated the relaxor state with nanoclusters as a polar glassy state, and the dielectric response of such an assembly is discussed in light of a relaxational model with frequency dependency. A static freezing temperature has been defined below which the polarization fluctuations cease and macroscopic polarization is restored. This temperature was reported as 291.5 K (18.5 °C) for PMN–10PT. The study by Song *et al.* (2005) on single crystal PMN–PT reports a similar temperature range where the polar nanoregion (PNR) state transforms into a metastable ferroelectric state with macrodomains, especially under an electric field. This temperature was observed at 18.3 °C for 0.90PMN–0.10PT single crystals. In our study, we have also observed a similar behavior from P–E hysteresis loops taken at different temperatures. Thus, the less inclined P–E hysteresis loops with higher P_r, P_{max}, and E_c values and a larger hysteresis that was observed at 0 °C can be attributed to the formation of a metastable ferroelectric state with macrodomains. A similar trend has also been observed in the case of textured ceramics for the P–E hysteresis loops measured at 0 °C and 25 °C.

When the P–E hysteresis loops of the random and textured ceramics in Fig. 4(a) were compared, below around T_m, it was

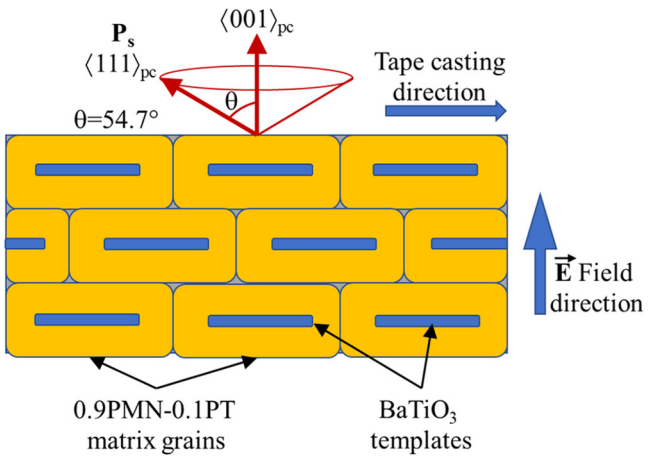

FIG. 5. Schematic drawing showing the orientational relationships in textured 0.90PMN–0.10PT.

observed regardless of the measurement temperature that random ceramics had higher P_r and P_{max} values and lower E_c values compared to the textured ceramics. This observation can be justified based on the development of a $\langle 001 \rangle_{pc}$ texture in a rhombohedrally distorted perovskite. The application of an electric field to 0.90PMN–0.10PT ceramics could be expected to induce a transition into a rhombohedral phase below T_m (Xu *et al.*, 2003). The spontaneous polarization direction in a perovskite with rhombohedral symmetry would be along the $\langle 111 \rangle_{pc}$ directions (Newnham, 2005). However, when a perovskite piezoceramic with rhombohedral symmetry is textured along $\langle 001 \rangle_{pc}$ direction, which is the case in 0.90PMN–0.10PT, then, as shown in the schematic drawing in Fig. 5, $P_{r\langle 001 \rangle}$ is expected to be $1/\sqrt{3}$ of the $P_{s\langle 111 \rangle}$, with an angle of 54.7° (Messing *et al.*, 2004; Yilmaz *et al.*, 2003; and Jin *et al.*, 2014), whereas in the case of random ceramics, the angles between P_r values of various grains and the $P_{s\langle 111 \rangle}$ vary from 0° to 54.7°. Thus, randomly oriented ceramics, when below T_m and in ferroelectric state, are expected to have higher P_r values on average compared to $\langle 001 \rangle_{pc}$ textured materials when the base symmetry is rhombohedral symmetry. This was clearly observed in the current study for temperatures up to around 20 °C, where P_r and P_{max} values of $\langle 001 \rangle_{pc}$ textured 0.90PMN–0.10PT ceramics were lower than that of the random 0.90PMN–0.10PT ceramics, as shown in Figs. 4(b) and 4(c). The polarization values obtained from P–E hysteresis measurements taken at various temperatures ranging from 90 °C to 0 °C are given in Figs. 6(a) and 6(b), respectively, for random and textured 0.90PMN–0.10PT ceramics. The decrease in polarization values could also be associated with hindered domain motion due to local constraints induced by the template BT crystals inside the grains. The increase that was observed in the case of E_c with texture, on the other hand, indicated that domain wall motion and polarization switching became more difficult. This might again be attributed to the clamping effect that arises from BT templates due to the existence of interfacial stresses. Examining Figs. 4(b) and 4(c) carefully, in the higher temperature regime (approximately >20 °C),

the textured sample displays a slightly higher P_r compared to the random sample in contrast to the $T < 20\,^{\circ}C$ range, which one can attribute to the BT template particles: as the BT crystallite templates are mostly ordered along their [001] directions, they can easily be poled by the field along the sample normal and remain so, yielding a remnant polarization slightly higher than the random samples keeping in mind that the BT volume is about 5% in the textured samples. Moreover, that BT templates are expected to polarize the surrounding regions of the nanoclusters in the PMN–PT matrix, when above T_m (~42 °C), is also going to add to the remnant polarization, and hence a slightly higher remanent polarization value compared to the random sample. At low temperatures ($T < T_m$), the volumetric polarization response will be dominated by the collective polarization of the PMN–PT that is in the ferroelectric state and therefore the BT template driven effects will be almost invisible, in accordance with the plots in Fig. 4. The P_{max} values for the random sample are, on average, higher than the textured samples that are likely due to the restricted domain wall mobility due to the BT templates in the latter as well as clamping effects.

Using the temperature dependent electrical measurements given in Fig. 6, we went on to estimate the EC response of the random and textured samples. The EC response, ΔT (change in temperature T) and isothermal entropy change, ΔS, of a system under thermodynamic equilibrium can be expressed as

$$\Delta S = -\int_{E_1}^{E_2} \left(\frac{\partial P}{\partial T}\right)_E dE, \tag{2}$$

$$\Delta T = T_f - T_o = -\int_{E_1}^{E_2} \frac{T}{C\rho}\left(\frac{\partial P}{\partial T}\right)_E dE, \tag{3}$$

between initial, E_1, and final, E_2, values of the electric field strength, E, where T_f, T_o, C, ρ, and $\left(\frac{\partial P}{\partial T}\right)_E$ are, respectively, the final temperature, initial temperature, heat capacity, density, and the pyroelectric coefficient of the material. The above equation relies on the Maxwell relation $\left(\frac{\partial S}{\partial E}\right)_T = \left(\frac{\partial P}{\partial T}\right)_E$ derived from the coefficient relations under adiabaticity, i.e., the pyroelectric coefficient is directly connected to the entropy changes under an applied field. The pyroelectric coefficient was determined using a portion of the upper branch of P vs E hysteresis loops for which $E \geq 0$ kV/cm. The derivative of P vs T data at constant E, i.e., the pyroelectric coefficient, was calculated in two different ways: (i) from the fourth order polynomial fits and (ii) from finite differences on a linear interpolator. In our calculations, C and ρ were taken as 0.34 J/g K and 8.13 g/cm^3, respectively.

Pyroelectric coefficient, ΔS vs T_o and ΔT vs T_o plots of random and $\langle 001 \rangle_{pc}$ textured 0.90PMN–0.10PT ceramics are given in Figs. 7(a)–7(c) and 7(d)–7(f), respectively. Additionally, a comparison of results based on different ways of determining the pyroelectric coefficient is also provided in Figs. 7(b) and 7(c) and 7(e) and 7(f) at several electric field strengths, E_2 and ($E_1 = 0$ kV/cm). It is clearly seen that results based on the use of polynomial fits are smooth in general but fail to capture depressions/peaks, for example, at $T_o = 20\,^{\circ}C$, emerging in the trends as the value of final electric field strength, E_2, increases. The ΔT values computed from

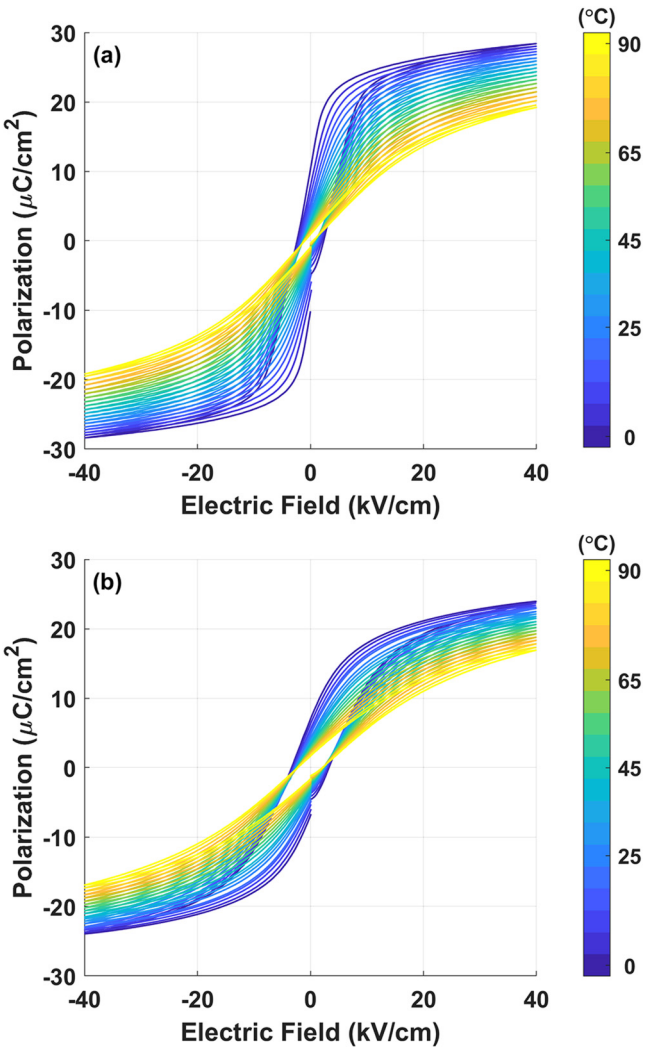

FIG. 6. Electric field induced polarization graphs of (a) random and (b) textured 0.90PMN–0.10PT samples measured at different temperatures.

the measurements of the random ceramics are comparable to the values reported in the literature (Valant, 2012 and Fulanovic *et al.*, 2017) for 0.90PMN–0.10PT bulk ceramics. The textured ceramic was found to have a lower ΔT within the measurement range. This result is consistent with the ferroelectric properties of the samples when the lower P–E hysteresis loops that were obtained from the textured ceramics compared to the random ones are considered. It is explainable within the same context using Fig. 5, i.e., the spontaneous polarization direction in a rhombohedral perovskite phase is along the $\langle 111 \rangle_{pc}$ direction and, thus, that would be the more preferable texturing direction for a polycrystalline ceramic. The studies on the anisotropic electrocaloric response of single crystals of 0.75PMN–0.25PT by Sebald *et al.* (2006) and 0.76PMN–0.24PT by Zhang *et al.* (2017) with rhombohedral symmetry along different

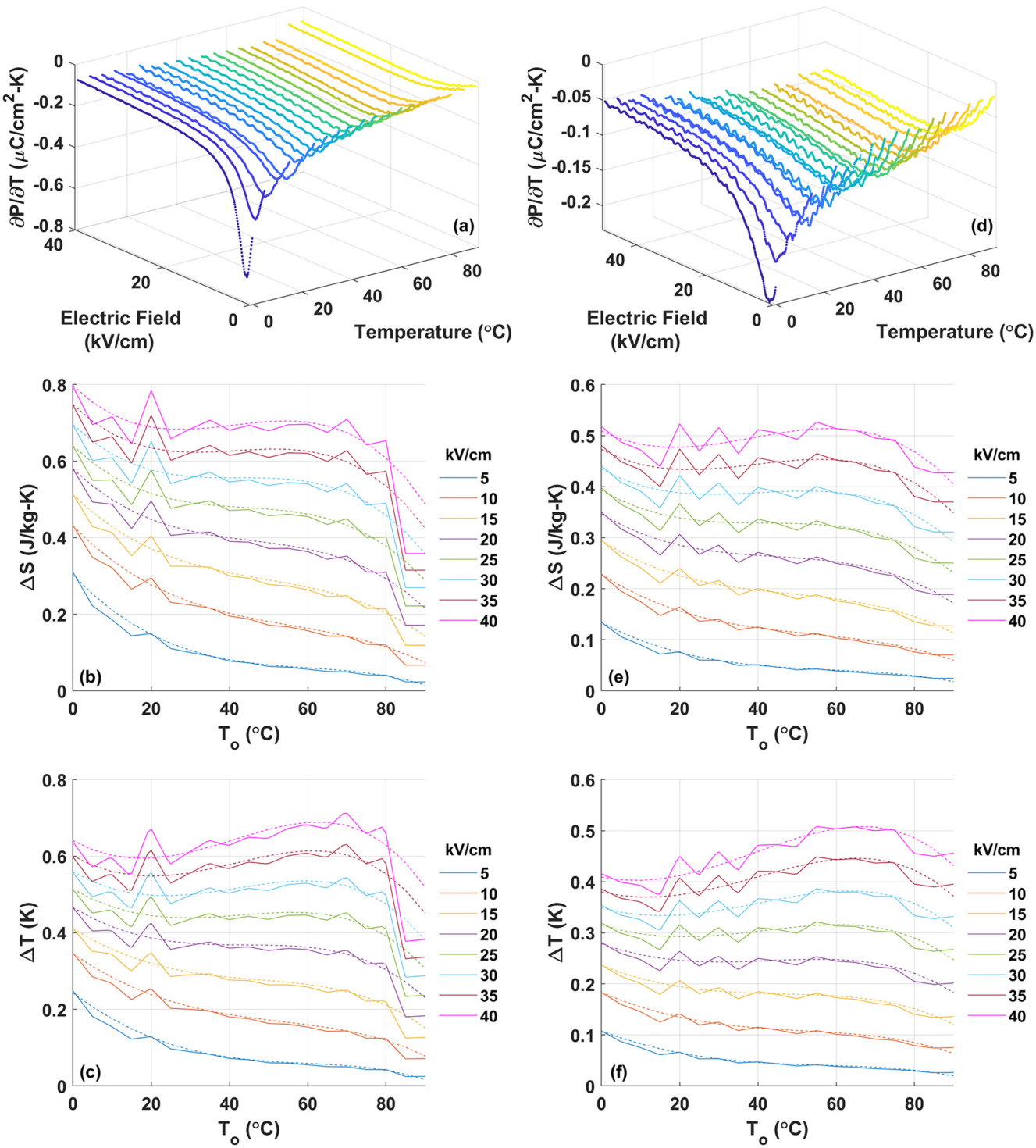

FIG. 7. (a) and (d) Pyroelectric coefficient, (b) and (e) ΔS vs T_o and (c) and (f) ΔT vs T_o plots of (a)–(c) random and (d)–(f) $\langle 001 \rangle_{pc}$ textured 0.90PMN–0.10PT ceramics. In (c), (d) and (e), (f) solid and dashed lines represent, at several electric field strengths, E_2 and (E_1 = 0 kV/cm), respectively, results based on use of pyroelectric coefficient determined via interpolation and fourth order polynomial fits.

crystallographic directions clearly demonstrated that crystals cut along the $\langle 111\rangle_{pc}$ directions have a visibly higher electrocaloric performance over the crystals cut along $\langle 110\rangle_{pc}$ and $\langle 100\rangle_{pc}$ directions. Among these three crystallographic directions, the $\langle 100\rangle_{pc}$ direction yielded the lowest ECE. When the results presented in Fig. 7 are evaluated within this context, it is clear that the preferred orientation to obtain higher electrocaloric performance from textured ceramics with rhombohedral symmetry should be the $\langle 111\rangle_{pc}$ direction, not the $\langle 001\rangle_{pc}$ direction. Texturing along the $\langle 001\rangle_{pc}$ direction does increase the piezoelectric properties drastically, compared to the random ceramics, as we also have previously observed in the PMN–32.5PT system (Berksoy-Yavuz *et al.*, 2018; 2019). However, since the BT templates with the tetragonal perovskite structure can usually be synthesized with major faces parallel to the (001) crystallographic planes, it does not seem possible to texture this material along $\langle 111\rangle_{pc}$. It might be possible to cut a $\langle 001\rangle_{pc}$ textured ceramic along specific directions, so that the poling direction is along [111]. As a final note, both the random and textured ceramics have a common feature where ΔT makes a plateau between 40 and 80 °C, which would make them rather useful for device applications in a wide temperature range, as expected of EC materials with a relaxor ferroelectric character. A similar behavior with matching amplitudes have been reported by Peräntie *et al.* (2013) where a broad region of maximal ΔT after around 20 °C, similar to the one observed in this paper, but with 20% higher max. amplitude under similar electric field levels, possibly due to the manner in which EC data were acquired.

In order to understand the impact of texture on the direct ECE of the composition of interest in this work, we have also carried out an analysis via the Landau theory of phase transitions. This would provide the primary EC response expected from the changes of the order parameter of the system, namely, electric polarization. The details of this analysis are presented in the supplementary material. The theoretically computed ΔT using the data in Fig. S5 in the supplementary material is given in Fig. 8. The transition for the bulk composition is around 36 °C that gives rise to the max. ΔT in this system. Note that the ΔT values, particularly near the transition, are more than two times than that estimated in our experiments for the textured sample. Moreover, ΔT estimated from experimental data has a positive slope in the 50–80 °C temperature regime and is oscillating around 0.7 °C for the random samples and 0.5 °C for the textured samples. Any experimental measurement of ΔT, whether directly or indirectly, is subject to secondary contributions such as strain and volume changes.

While it is quite difficult to distinguish the secondary contributions from the primary ECE driven by the $\frac{\partial P_s}{\partial T}$ term in Eq. (3), it has very recently been discussed, in a detailed study by Pandya *et al.* (2019) focusing on films, that secondary effects can in fact become a major factor in the overall pyroelectric response, degrading the maximum achievable temperature changes in these systems. In a study by Velarde *et al.* (2019), Zr-rich rhombohedral compositions of Pb,Zr,TiO_3 have been shown to exhibit a very strong secondary pyroelectric coefficient contribution that was shown to be detrimental to the overall ECE in these materials compared to the Ti-rich compositions. Indeed, following the comparison of the measurements on the $\langle 001\rangle_{pc}$ textured sample with that of predicted from theory here, it is surprising to observe a two to three

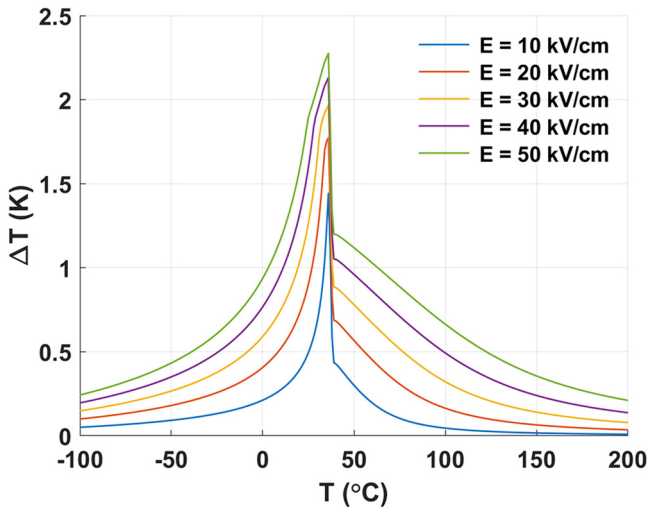

FIG. 8. Electrocaloric effect ΔT vs T_o of 0.90PMN–0.10PT for several values of $\vec{E} \parallel [001]$.

times difference between the computed primary max. ΔT and the experimentally estimated value. Apart from smearing effects that the pyroelectric coefficient undergoes due to internal bias fields and defects in real samples, the numbers reported from experimental work here are in close proximity to that reported earlier in the literature (Valant, 2012 and Fulanovic *et al.*, 2017). Keeping in mind that the thermodynamic potential constructed to compute the primary ΔT in our study produces the equilibrium phases and stable polarization components of the 0.90PMN–0.10PT system (Heitmann and Rosetti, 2014; Khakpash *et al.*, 2015), we infer that the secondary effects going into ΔT are rather significant for this system. Moreover, as thermodynamic theory excludes melting of the ferroelectric phase into polar nanoregions and such for equilibrium considerations, the computed values of ΔT from thermodynamic theory given above or around the peak value are expected to be higher than the real measurements on relaxors (see Hagberg *et al.*, 2008 and Peräntie *et al.*, 2013). A peak value of $\Delta T \cong 0.55\,^{\circ}C$ has been observed by Hagberg *et al.* (2008) around the depolarization temperature for the powder sintered 87PMN–13PT composition that is close to the magnitude we report here for the random oriented samples. Our systematic measurements on textured and random oriented samples demonstrate that texturing along the [001] direction in the composition investigated here does not produce an enhancement in ΔT. Despite the premise of the thermodynamic theory, the visible variation of the ΔT in the textured and the random samples can be used as an argument to corroborate that polar nanoregions "feel" a restriction by the templates, circumstancing a lower ΔT. This is indeed consistent with the relative loss of hysteresis, i.e., the lower P_r and P_{max} values in the textured samples, also pointing out to a weaker pyroelectric response under an applied field. The reason for the decreased hysteresis has been discussed in a relevant section in Fig. 4. Albeit reported for films and multilayers, reduced domain mobility has

been shown to lead to the degradation of the pyroelectric response, which in turn should be expected to lead to lowering of the ΔT in these systems (Misirlioglu *et al.*, 2014). From another perspective, however, one should also realize that the measurement of a "pyroresponse induced current in a capacitor setting" coming from domain wall motion is different than a scalar change in polarization magnitude inside the lattice due to temperature changes and the ECE depends on the latter. We, therefore, conclude that texturing could also reduce the ECE via amplifying the secondary, i.e., piezoelectric contributions to ΔT through enhanced piezoelectric activity.

As the ECE is rather complexly coupled (an integral function of the pyroelectric response as a function of electric field), it was intuitively thought that engineering the pyroelectric response through template crystals would have a positive enhancement, and hence a higher ECE in a textured specimen than in the one whose grains are randomly oriented. In this work, we have reported our intention and motivation to start the study keeping in mind the above points. However, enhancing a specific property is not always the final outcome of texturing and the ECE turns out to be as such for texturing along $\langle 001 \rangle_{pc}$. The possible mechanisms behind such an outcome have been discussed, which we think would serve as a valuable input to the ongoing works of other groups active in device design tailoring the ECE. It was our conclusion that texturing a relaxor system with rhombohedral symmetry along $\langle 111 \rangle_{pc}$ would be a viable way to enhance the ECE. Additionally, possible secondary mechanisms have also been mentioned that could be detrimental to the observed ECE, not accounted for in earlier reports. Comparison with thermodynamic theory has also been done to highlight the possible presence of such secondary mechanisms that could be taking place as discussed in the text.

IV. CONCLUSIONS

We synthesized random and $\langle 001 \rangle_{pc}$ textured 0.90PMN–0.10PT samples where we used BT single crystal templates. Structural data reveal that the samples possess a pseudocubic crystalline structure rather than a rhombohedral one as we cannot detect the peak splittings expected in the latter. Electrical measurements reveal that texturing causes a slanting and loss in the hysteresis with respect to the randomly oriented samples in a wide temperature range. Temperature dependent dielectric measurements display a reduction in the maxima of the dielectric constant near the transition, and texturing has not shifted the transition temperature to the paraelectric state deduced from the position of the maxima regardless of measurement frequency. The Curie–Weiss analysis show that the γ coefficients extracted from curve fits are consistent with a relaxor type behavior. We estimated the ECE from the experimental data available and observed that textured samples have a lower ΔT compared to the randomly oriented samples possibly due to the non-preferable texture direction, which causes a decrease in the ferroelectric properties as well as the constraints induced by the template particles. In order to understand the extent to which the secondary effects might govern the ECE, we carried out a thermodynamic analysis using the Landau theory of phase transitions with the phenomenological coefficients acquired from published data in the literature for the composition of interest. There is about two to three times difference between the theoretically calculated single crystal ECE and that of experimentally measured for the system studied here including previous reports. Experimental data shows that texturing these structures along $\langle 001 \rangle_{pc}$, while good for some of the properties such as the piezoelectric coefficient, might not be an effective option to enhance the ECE.

SUPPLEMENTARY MATERIAL

See the supplementary material for further analysis of the modified Curie–Weiss behavior and the details of the analysis of the system via Landau theory of phase transitions.

ACKNOWLEDGMENTS

The authors would also like to acknowledge the financial support of AFOSR through Grant No. FA9550-18-1-0450.

DATA AVAILABILITY

The data that support the findings of this study are available from the corresponding author upon reasonable request.

REFERENCES

Berksoy-Yavuz, A. and Mensur-Alkoy, E., "Electrical properties and impedance spectroscopy of crystallographically textured 0.675[$Pb(Mg_{1/3}Nb_{2/3})O_3$]-0.325[$PbTiO_3$] ceramics," J. Mater. Sci. Mater. Electron. **29**, 13310 (2018).

Berksoy-Yavuz, A., Mensur-Alkoy, E., Gozutok, E., Dursun, S., Yılmaz, H., and Alkoy, S., "Structural and electrical properties of (001) textured 0.26PIN-0.40PMN-0.34PT ternary system," J. Mater. Sci. Mater. Electron. **30**, 18548–18556 (2019).

Bokov, A. A., Bing, Y.-H., Chen, W., Ye, Z.-G., Bogatina, S. A., Raevski, I. P., Raevskaya, S. I., and Sahkar, E. V., "Empirical scaling of the dielectric permittivity peak in relaxor ferroelectrics," Phys. Rev. B **68**, 052102 (2003).

Bokov, A. A., Luo, H., and Ye, Z.-G., "Polar nanodomains and relaxor behaviour in (1−x)$Pb(Mg_{1/3}Nb_{2/3})O_3$–x$PbTiO_3$ crystals with x=0.3–0.5," Mater. Sci. Eng. B **120**, 206–209 (2005).

Burns, G. and Dacol, F. H., "Crystalline ferroelectrics with glassy polarization behavior," Phys. Rev. B **28**, 2527–2530 (1983).

Cakmak, O., Mensur-Alkoy, E., Toprak, G., Tuna, O., and Alkoy, S., "Investigation of the electrical properties of textured 0.5[$Ba(Zr_{0.2}Ti_{0.8})$]O_3-0.5[$(Ba_{0.7}Ca_{0.3})TiO_3$] piezoceramics," J. Mater. Sci Mater. Electron. **31**, 4184–4192 (2020).

Cross, L. E., "Relaxor ferroelectrics," Ferroelectrics **76**, 241–267 (1987).

Dai, X., Xu, Z., and Viehland, D., "The spontaneous relaxor to normal ferroelectric transformation in La-modified lead zirconate titanate," Philos. Mag. B **70**, 33–48 (1994).

Fulanovic, L., Drnovsek, S., Ursic, H., Vrabelj, M., Kuscer, D., Makarovic, K., Bobnar, V., Kutnjak, Z., and Malic, B., "Multilayer 0.9$Pb(Mg_{1/3}Nb_{2/3})O_3$–0.1$PbTiO_3$ elements for electrocaloric cooling," J. Eur. Ceram. Soc. **37**, 599–603 (2017).

Gehring, P. M., Chen, W., Ye, Z. G., and Shirane, G., arXix:cond-mat/0304289 (2003).

Goupil, F. L., Axelsson, A. K., Dunne, L. J., Valant, M., Manos, G., Lukasiewicz, T., Dec, J., Berenov, A., and Alford, N. M., "Anisotropy of the electrocaloric effect in lead-free relaxor ferroelectrics," Adv. Energy Mater. **4**, 1301688 (2014).

Greco, A., Aprea, C., Maiorino, A., and Masselli, C., "A review of the state of the art of solid-state caloric cooling processes at room-temperature before 2019," Int. J. Refrig. **106**, 66–88 (2019).

Hagberg, J., Uusimäki, A., and Jantunen, H., "Electrocaloric characteristics in reactive sintered 87Pb($Mg_{1/3}Nb_{2/3}$)O_3–0.13 $PbTiO_3$," Appl. Phys. Lett. **92**, 132909 (2008).

Heitmann, A. and Rossetti, G. A., "Thermodynamics of ferroelectric solid solutions with morphotropic phase boundaries," J. Am. Ceram. Soc. **97**, 1661–1685 (2014).

Hino, T., Sugioka, T., Tamura, S., Nishida, M., and Araki, T., "Diffuse phase transition in Ba(Sn_xTi_{1-x}) ceramics and thin films," J. Laser Micro/Nanoeng. **6**(2), 119–123 (2011).

Jin, L., Li, F., and Zhang, S., "Decoding the fingerprint of ferroelectric loops: Comprehension of the material properties and structures," J. Am. Ceram. Soc. **97**, 1–27 (2014).

Kaya, M. Y., Mensur-Alkoy, E., Gurbuz, A., Oner, M., and Alkoy, S., "Influence of compositional variation on the electrical properties of [Pb($Zn_{1/3}Nb_{2/3}$)O_3]-[Pb(Zr,Ti)O_3] ceramics and their transducer application," IEEE Trans. Ultrason. Ferroelectr. Freq. Control **65**, 1268–1277 (2018).

Khakpash, N., Khassaf, H., Rossetti, G. A., and Alpay, S. P., "Misfit strain phase diagrams of epitaxial PMN–PT films," Appl. Phys. Lett. **106**, 082905 (2015).

Liu, D., Yan, Y., and Zhou, H., "Synthesis of micron-scale platelet $BaTiO_3$," J. Am. Ceram. Soc. **90**, 1323–1326 (2007).

Liu, G., Kong, L., Hu, Q., and Zhang, S., "Diffused morphotropic phase boundary in relaxor-$PbTiO_3$ crystals: High piezoelectricity with improved thermal stability," Appl. Phys. Rev. **7**, 021405 (2020).

Lotgering, F. K., "Topotactical reactions with ferrimagnetic oxides having hexagonal crystal structures—I," J. Inorg. Nucl. Chem. **9**, 113–123 (1959).

Lu, S. G., Rožič, B., Zhang, Q. M., Kutnjak, Z., Li, X., Furman, E., Gorny, L. J., Lin, M., Malič, B., Kosec, M., Blinc, R., and Pirc, R., "Organic and inorganic relaxor ferroelectrics with giant electrocaloric effect," Appl. Phys. Lett. **97**, 162904 (2010).

Messing, G. L., Poterela, S., Chang, Y., Frueh, T., Kupp, E. R., Watson, B. H., Walton, R. L., and Brova, M. J., "Texture-engineered ceramics—Property enhancements through crystallographic tailoring," J. Mater. Res. **32**, 3219–3241 (2017).

Messing, G. L., Trolier-McKinstry, S., Sabolsky, E. M., Duran, C., Kwon, S., Brahmaroutu, B., Park, P., Yılmaz, H., Rehrig, P. W., Eitel, K. B., Suvaci, E., Seabaugh, M., and Oh, K. S., "Templated grain growth of textured piezoelectric ceramics," Crit. Rev. Solid State Mater. Sci. **29**, 45–96 (2004).

Mischenko, A. S., Zhang, Q., Scott, J. F., Whatmore, R. W., and Mathur, N. D., "Giant electrocaloric effect in thin-film $PbZr_{0.95}Ti_{0.05}O_3$," Science **311**, 1270–1271 (2006).

Misirlioglu, I. B., Kesim, M. T., and Alpay, S. P., "Layer thickness and period as design parameters to tailor pyroelectric properties in ferroelectric superlattices," Appl. Phys. Lett. **105**, 172905 (2014).

Newnham, R. E., *Properties of Materials Anisotropy, Symmetry, Structure* (Oxford University Press, 2005), pp. 58–71.

Pandya, S., Velarde, G. A., Gao, R., Everhardt, A. S., Wilbur, J. D., Xu, R. J., Maher, J. T., Agar, J. C., Dames, C., and Martin, L. W., "Understanding the role of ferroelastic domains on the pyroelectric and electrocaloric effects in ferroelectric thin films," Adv. Mater. **31**, 1803312 (2019).

Peräntie, J., Tailor, H. N., Hagberg, J., Jantunen, H., and Ye, Z.-G., "Electrocaloric properties in relaxor ferroelectric (1-x)Pb($Mg_{1/3}Nb_{2/3}$)O_3–x$PbTiO_3$ system," J. Appl. Phys. **114**, 174105 (2013).

Qian, X. S., Ye, H. J., Zhang, Y. T., Gu, H., Li, X., Randall, C. A., and Zhang, Q. M., "Giant electrocaloric response over a broad temperature range in modified $BaTiO_3$ ceramics," Adv. Funct. Mater. **24**, 1300–1305 (2014).

Richter, T., Denneler, S., Schuh, C., Suvaci, E., and Moos, R., "Textured PMN–PT and PMN–PZT," J. Am. Ceram. Soc. **91**, 929–933 (2008).

Sanlialp, M., Shvartsman, V. V., Acosta, M., and Lupascu, D. C., "Electrocaloric effect in Ba(Zr,Ti)O_3–(Ba,Ca)TiO_3 ceramics measured directly," J. Am. Ceram. Soc. **99**, 4022–4030 (2016).

Sebald, G., Seveyrat, L., Guyomar, D., Lebrun, L., Guiffard, B., and Pruvost, S., "Electrocaloric and pyroelectric properties of 0.75Pb($Mg_{1/3}Nb_{2/3}$)O_3–0.25$PbTiO_3$ single crystal," J. Appl. Phys. **100**, 124112 (2006).

Shvartsmana, V. V. and Kholkin, A. L., "Evolution of nanodomains in 0.9P$bMg_{1/3}Nb_{2/3}O_3$-0.1$PbTiO_3$ single crystals," J. Appl. Phys. **101**, 064108 (2007).

Song, P., Wang, H. X., and Luo, H. S., "Dependence of dielectric properties of 0.9Pb($Mg_{1/3}Nb_{2/3}$)O_3-0.1$PbTiO_3$ crystals on the crystallographic orientation and external electric field," Ferroelectrics **322**, 39–43 (2005).

Uchino, K. and Nomura, S., "Critical exponents of the dielectric constants in diffused-phase-transition crystals," Ferroelectrics **44**, 55–61 (1982).

Valant, M., "Electrocaloric materials for future solid-state refrigeration technologies," Prog. Mater. Sci. **57**, 980–1009 (2012).

Velarde, G., Pandya, S., Zhang, L., Garcia, D., Lupi, E., Gao, R., Wilbur, J. D., Dames, C., and Martin, L. W., "Quantifying intrinsic, extrinsic, dielectric, and secondary pyroelectric responses in $PbZr_{1-x}Ti_xO_3$ thin films," ACS Appl. Mater. Interfaces **11**, 35146–35154 (2019).

Viehland, D., Jang, S. J., Cross, L. E., and Wuttig, M., "Freezing of the polarization fluctuations in lead magnesium niobate relaxors," J. Appl. Phys. **68**, 2916–2921 (1990).

Vrabelj, M., Ursic, H., Kutnjaka, Z., Rozic, B., Drnovsek, S., Bencan, A., Bobnar, V., Fulanovic, L., and Malic, B., "Large electrocaloric effect in grain-size-engineered 0.9Pb($Mg_{1/3}Nb_{2/3}$)O_3–0.1$PbTiO_3$," J. Eur. Ceram. Soc. **36**, 75–80 (2016).

Wang, H., Xu, H., Luo, H., Yin, Z., Bokov, A. A., and Ye, Z. G., "Dielectric anomalies of the relaxor-based 0.9Pb($Mg_{1/3}Nb_{2/3}$)O_3-0.1$PbTiO_3$ single crystals," Appl. Phys. Lett. **87**, 012904 (2005).

Xu, G., Viehland, D., Li, J. F., Gehring, P. M., and Shirane, G., "Evidence of decoupled lattice distortion and ferroelectric polarization in the relaxor system PMN-xPT," Phys. Rev. B **68**, 212410 (2003).

Yilmaz, H., Trolier-McKinstry, S., and Messing, G. L., "(Reactive) templated grain growth of textured sodium bismuth titanate ($Na_{1/2}Bi_{1/2}TiO_3$-$BaTiO_3$) ceramics—II Dielectric and piezoelectric properties," J. Electroceram. **11**, 217–226 (2003).

Yimnirun, R., "Dielectric properties of lead magnesium niobate–lead titanate ceramics prepared by mixed oxide method," Int. J. Mod. Phys. B **23**, 403–410 (2009).

Zhang, T. F., Tang, X. G., Ge, P. Z., Liu, Q. X., and Jiang, Y. P., "Orientation related electrocaloric effect and dielectric phase transitions of relaxor PMN-PT single crystals," Ceram. Int. **48**, 16300–16305 (2017).